PHYSICAL REVIEW B VOLUME 27, NUMBER 3 1 FEBRUARY 1983

Thermoreflectance investigation of the antiferromagnetic and paramagnetic phases of Cr

E. Colavita and A. Franciosi
Istituto di Fisica G. Marconi, Università di Roma, Rome, Italy
and Dipartimento di Fisica, Università della Calabria, Arcavacata di Rende, Cosenza, Italy

D. W. Lynch
Ames Laboratory and Department of Physics, Iowa State University, Ames, Iowa 50011

G. Paolucci and R. Rosei
Istituto di Fisica G. Marconi, Università di Roma, Rome, Italy
and Dipartimento di Fisica, Università della Calabria, Arcavacata di Rende, Cosenza, Italy
(Received 15 June 1982)

Thermoreflectance measurements have been performed on Cr single crystals at several temperatures above and below the Néel temperature. We observe dramatic changes induced by the magnetic phase transition. In contrast, static optical data fail to show appreciable differences in the (0.5—5.0)-eV photon-energy range. Magnetic ordering gives rise to the disappearance of transitions involving specific regions of the Fermi surface. New critical-point absorptions appear at the boundaries of the new Brillouin zone in antiferromagnetic Cr. Most of the observed experimental features have been identified by comparison with recent band-structure calculations.

I. INTRODUCTION

Chromium has been studied intensively since it was suggested that its ground state below the Néel temperature ($T_N = 312$ K) contains a spin-density wave.[1–13] Neutron-diffraction measurements have shown that the antiferromagnetic spin arrangement does not have exactly twice the periodicity of the lattice, which is expected for a simple antiferromagnetic array of magnetic moments on lattice sites.[14] The difference between the magnetic moment and the lattice periodicities depends on temperature, and it can be altered by alloying. The commensurate antiferromagnetic structure is stabilized by the addition of about 1% Mn to Cr.[15] The ground state of antiferromagnetic pure Cr is, however, very close to that of the commensurate phase found in alloys. Band structures have been calculated for both paramagnetic Cr (Refs. 5, 11, and 16–21) and (hypothetical) commensurate antiferromagnetic Cr (Refs. 5, 22, and 23). In the following discussion we refer to this hypothetical state when referring to antiferromagnetic Cr.[24]

The magnetic phase transition produces energy gaps at the Fermi level at certain points in the Cr paramagnetic Brillouin zone (BZ) due to band rehybridization.[23] Moreover, the bcc BZ for Cr in the paramagnetic state must be replaced in the antiferromagnetic state by a new zone which is simple cubic.[25]

Infrared-absorption measurements demonstrated the formation of gaps in the band structure.[6–9] Transitions across the gaps are electric dipole allowed and they give rise to easily detected absorption peaks. In incommensurate pure Cr such a gap occurs at about 0.13 eV, while in dilute Cr-based commensurate antiferromagnetic alloys the gap is at 0.4 eV. This difference is understood, and the gap referred to is the gap caused by the exchange potential of the spin-density wave.[12] Later measurements[10] showed that there was a second infrared-absorption peak in antiferromagnetic pure Cr which followed the temperature dependence of the spin-density-wave magnitude. It was ascribed to an indirect transition across a double gap, similar to the gap occurring in commensurate Cr alloys. At higher energies there is a region of strong interband optical absorption. At such energies, of the order of 1 eV, absorption across the gaps caused by the ordering does not occur, for the gaps are too small, but transitions do occur whose initial or final states, but not both, may be shifted upon the formation of a gap produced by magnetic ordering. Because of the overlapping interband transitions, some of which are not expected to be influenced by magnetic ordering, the effect of ordering upon these transitions is difficult to study in static optical measurements, and no such effects were seen.[8] Thermomodulation spectroscopy is uniquely suited for studying such effects. It greatly enhances contributions from optical tran-

sitions to and from the Fermi surface.[26,27] Moreover, it is especially suitable[28,29] for detecting new critical points which may occur at the boundaries of the antiferromagnetic BZ. We show that this is indeed the case, and we report below a study on the temperature dependence of the interband transitions not previously studied. (Angle-resolved photoemission is used frequently in the study of the electronic structure of solids, but there has been to date only one application to Cr.[30] The $\langle 110 \rangle$ direction in the Brillouin zone was studied, and some effects of magnetic ordering were observed. The results were generally consistent with the band structure calculated by Asano and Yamashita,[5] but a detailed "experimental" band structure was not determined. The photoemission results were consistent with what we report below, but a direct comparison cannot be made.)

We present here a thermoreflectance investigation of the antiferromagnetic-to-paramagnetic phase transition in Cr single crystals. Measurements taken in the (0.5—5.0)-eV photon-energy range, above and below the Néel temperature, reveal dramatic modifications of the optical spectrum with magnetic ordering. The changes are directly related to the destruction of portions of the Fermi surface[21,31] and this allowed us to identify unambiguously specific regions in $\vec{k}$ space which account for major contributions to the optical absorption. Furthermore, we were able to relate several Cr-absorption features to transitions at specific critical points in the antiferromagnetic BZ. An M_1 and several M_3 critical points were found to disappear in the paramagnetic phase. The results of recent band-structure calculations[23] were compared with theoretical thermoreflectance line shapes[32] obtained with a simplified analytical model,[32,33] and the remarkably good agreement with experiment substantiates our identifications.

II. EXPERIMENTAL

The sample was a thin single-crystal slab ($2\times3\times0.2$ mm^3) cut with a low-speed diamond saw and polished with abrasives. Mechanical damage was removed by electropolishing with 6% perchloric acid in methanol at dry-ice temperature. The sample was then mounted with a very thin layer of diluted Duco cement onto the heater which in turn was held on the cold tip of a cryostat.

The temperature modulation was obtained by passing a unipolar current wave through the heater. The measurements at low temperature were done with the use of a highly efficient modulation arrangement extensively tested[34] and liquid nitrogen as a refrigerant in the cryostat. The heater in this case was a metal film evaporated on a thin sapphire substrate. The power dissipated in the heater increased the average temperature of the sample to about 190 K (as measured with a differential thermocouple on a mock sample in a separate run).

The measurements at, or above, room temperature were done with the use of a thin silicon slab as a heater and the cryostat was cooled with circulating water. This modulation arrangement is sturdier but less efficient: The peak-to-peak temperature oscillation of the sample was estimated to be ~1 K with a power dissipation of 5 W at 1 Hz.

The ac thermal excursion of the samples scales all spectra and results in arbitrary amplitudes, different for each sample mounting and for different heat-sink temperatures. This is not important, however, for we consider only the shape of the spectra.

The relative temperature-induced change in the reflectance $\Delta R/R$ was measured through digital integration of the lock-in amplifier output at each photon energy. Integration times up to several hundred seconds for high-temperature measurements and of 20—30 sec at low temperature were necessary to reduce the statistical uncertainty below 3% over the whole energy range. The high-energy region (3.8—5.0 eV) of the spectrum carries a higher statistical uncertainty (10%). Details of the experimental heater, electronics, and data handling have been described elsewhere.[35]

III. DATA OVERVIEW

The thermoreflectance spectra of Cr single crystals taken at several different temperatures ($T=325$, 303, and 192 K) are shown in Fig. 1. For comparison, Fig. 1 also shows the thermoreflectance spectrum of a Cr film at 80 K taken from Ref. 36.

The structures around 1 eV change appreciably with temperature while those around 2 eV have a less dramatic, but constant, evolution. All the other higher-energy structures are quite unaffected by the temperature change. We observe that on going from the paramagnetic to the antiferromagnetic phase the modification is not abrupt with temperature but is completed at 192 K.[37] The spectrum taken at 325 K is very similar, but not identical, to the spectrum for evaporated Cr films, which are probably representative of the paramagnetic state, as we will discuss in the following sections. As can be seen, the structures around 2.25 eV become less evident at 325 K and seem to disappear only in the Cr-film data.

Thermoreflectance spectra are difficult to interpret by themselves, for they contain structures influenced by both the real and imaginary parts of the dielectric function and its temperature-induced change $\Delta\tilde{\epsilon}$ with specific interband transitions. Thus the $\Delta R/R$ spectra have been Kramers-Kronig (KK)

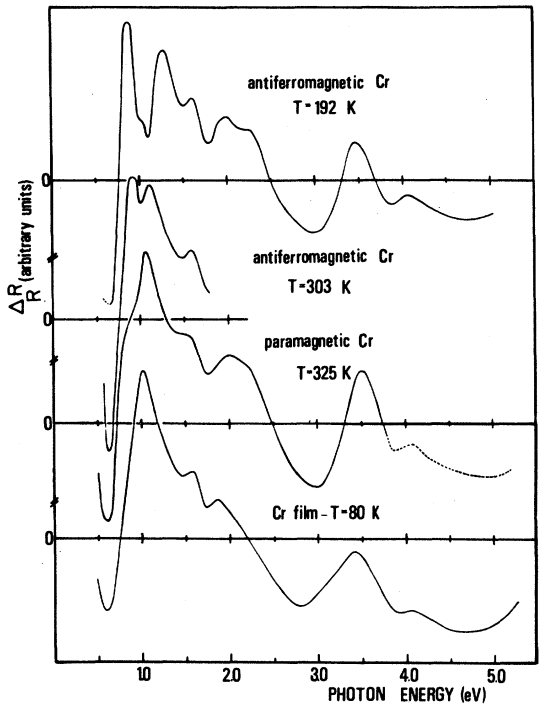

FIG. 1. Thermoreflectance $\Delta R/R$ spectra of Cr single crystals. From top: average sample temperature $\bar{T}=325$, 303, and 192 K. Lowest curve: thermoreflectance spectrum of a Cr film at $\bar{T}=80$ K, from Weaver *et al.* (Ref. 36). The film spectrum seems clearly representative of the paramagnetic state of Cr.

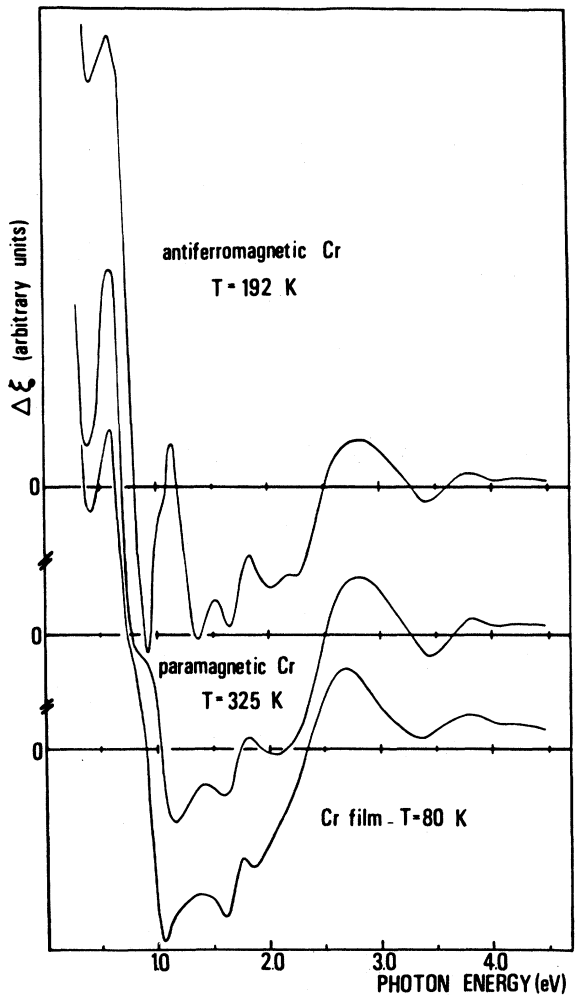

FIG. 2. Modulation $\Delta\epsilon_1$ of the real part of the dielectric function $\tilde{\epsilon}=\epsilon_1+i\epsilon_2$ for Cr metal. From top: bulk sample at $\bar{T}=192$ K; bulk sample at 325 K. Lowest curve: Cr film at 80 K. The spectra were obtained through Kramers-Kronig analysis of the $\Delta R/R$ data of Fig. 1 and of Ref. 36. Low-temperature static $\tilde{\epsilon}$ data from Ref. 9 were used for the analysis in all cases since $\tilde{\epsilon}$ shows very little temperature dependence (Ref. 39).

analyzed in order to obtain the temperature-induced change in the phase shift of the reflected electric field. This analysis requires an extrapolation of the $\Delta R/R$ data to zero and infinite energies, but for derivative spectra such as ours the results of KK analysis are not very sensitive to these extrapolations.[38] The computation of $\Delta\tilde{\epsilon}$ also requires values of the dielectric function $\tilde{\epsilon}$, which were obtained from Ref. 9. The use of low-temperature static $\tilde{\epsilon}$ data for the analysis of modulated spectra at different temperatures is justified since $\tilde{\epsilon}$ shows very little temperature dependence.[39]

Figure 2 shows $\Delta\epsilon_1$ spectra of Cr at 192 and 325 K. Also shown for comparison is the $\Delta\epsilon_1$ spectrum for a Cr film, calculated from the data of Ref. 36. Figure 3 shows the corresponding $\Delta\epsilon_2$ spectra. Again, the low-energy part of the spectra shows dramatic differences on changing the magnetic ordering, while the higher-energy range (above 2.7 eV) is relatively unaffected.

IV. CHROMIUM ELECTRONIC STRUCTURE

Recently, a complete self-consistent band-structure calculation for the hypothetical commensurate antiferromagnetic phase of Cr has been calculated by Skriver.[23] We will interpret our low-temperature data with this band structure,[24] shown in Fig. 4. Several calculations exist for paramagnetic Cr.[5,11,16–21] In Fig. 5 we show results taken from Ref. 31. The paramagnetic bcc BZ is shown in Fig. 6 (heavy solid lines) together with the CsCl BZ of commensurate antiferromagnetic Cr (thin solid lines). The irreducible parts of the BZ are also sketched (dotted and dashed lines, respectively) in Fig. 6.

In the superlattice of the CsCl structure the eigenspace $\{\vec{K}\}$ consists of the eigenspace of $\{\vec{K}\}$ and of

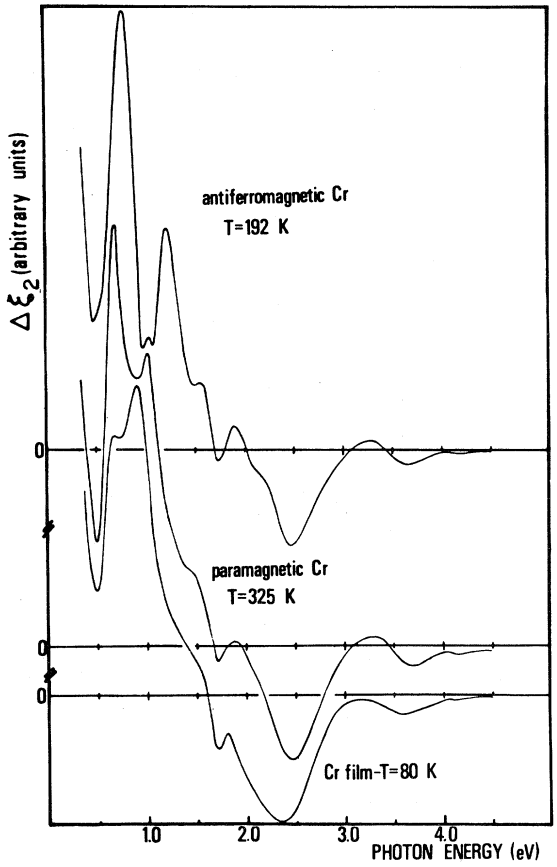

FIG. 3. Modulation $\Delta\epsilon_2$ of the imaginary part of the dielectric function $\tilde{\epsilon}=\epsilon_1+i\epsilon_2$ for Cr. From top: bulk sample at $\bar{T}=192$ K; bulk sample at 325 K. Lowest curve: Cr film at 80 K. The spectra were obtained from Kramers-Kronig analysis of the $\Delta R/R$ data of Fig. 1 and Ref. 36. Low-temperature static $\tilde{\epsilon}$ data from Ref. 9 were used for the analysis in all cases since $\tilde{\epsilon}$ shows very little temperature dependence (Ref. 39).

$\{\vec{K}+\vec{Q}\}$ of the bcc structure, where $\vec{K}$ is the crystal momentum and $\vec{Q}=(2\pi/a)(0,0,1)$ is the wave vector of the spin-density wave. A rough picture (Fig. 7) of the band structure for the antiferromagnetic state can be obtained by folding back the bands

TABLE I. Possible candidates for the interband transitions involving the Fermi surface observed at 0.9, 1.4, and 1.6 eV in antiferromagnetic Cr (see sketch in Fig. 9). These are derived from the band diagram of Fig. 4 through selection-rule and joint-density-of-states arguments.

Energy (eV)	Optical transitions
0.9	$\Sigma_4\rightarrow\Sigma_1$, $\Sigma_1\rightarrow\Sigma_1$, $\Sigma_4\rightarrow\Sigma_1$, $S_4\rightarrow S_1$, $T_5\rightarrow T_1$, $T_1\rightarrow T_2$
1.4	$\Sigma_4\rightarrow\Sigma_1$, $\Sigma_1\rightarrow\Sigma_4\rightarrow T_5\rightarrow T_2$, $S_2\rightarrow S_3$
1.6	$\Sigma_1\rightarrow\Sigma_4$, $\Sigma_1\rightarrow\Sigma_3$, $T_5\rightarrow T_1$

of the paramagnetic state into the simple cubic BZ. This procedure is quite useful for understanding the origin of the energy levels in the antiferromagnetic band structure. By comparing Figs. 4 and 7 it appears that upon turning on the antiferromagnetic interaction, new gaps open at the surface of the new BZ and accidental degeneracies are removed through the opening of energy gaps along the Λ and Σ axes (near the Fermi surface). Figure 7 also indicates that several energy levels are largely unaffected by the phase transition, which accounts for the similarities of the density of states[23,31] and static optical spectra of antiferromagnetic[9] and paramagnetic Cr.[40]

Figure 8 [panels (a) and (b)] shows all the allowed critical-point transitions at high-symmetry points which should occur in antiferromagnetic and paramagnetic Cr. The same figure [panels (c) and (d)] also shows the most important[41] Fermi-surface interband transitions which should be affected by magnetic ordering (along the Δ, G, and Λ symmetry lines). The arrows indicate Fermi-surface and critical-point transitions determined experimentally (see following paragraphs).

V. DISCUSSION

A. The antiferromagnetic phase

The $\Delta\epsilon_2$ spectrum of antiferromagnetic Cr in Fig. 3 exhibits three sharp structures in the (0.5—1.8)-eV

TABLE II. Fitting parameters used in the analytical fitting of the $\Delta R/R$ spectrum of antiferromagnetic Cr at 192 K (see Fig. 11). The energy location of the critical points is reliable to within ± 0.01 eV and the broadening parameters to within $\pm 3\%$. W is a phenomenological weight parameter proportional to $J(\Gamma)^{-1/2}|M|^2|\Delta E_0|$, where J is a topological factor, ΔE_0 is the temperature-induced variation of the energy gap, and M is the transition matrix element. Not too much physical significance, however, should be attached to this parameter.

Critical point	M_1	M_2	M_3	M_0	M_2	M_3
Onset E_0 (eV)	1.95	2.37	2.65	3.03	3.48	3.72
Broadening Γ (eV)	0.13	0.12	0.24	0.22	0.15	0.10
Weight W (eV^2)	1.45	2.29	2.35	1.63	1.74	0.66

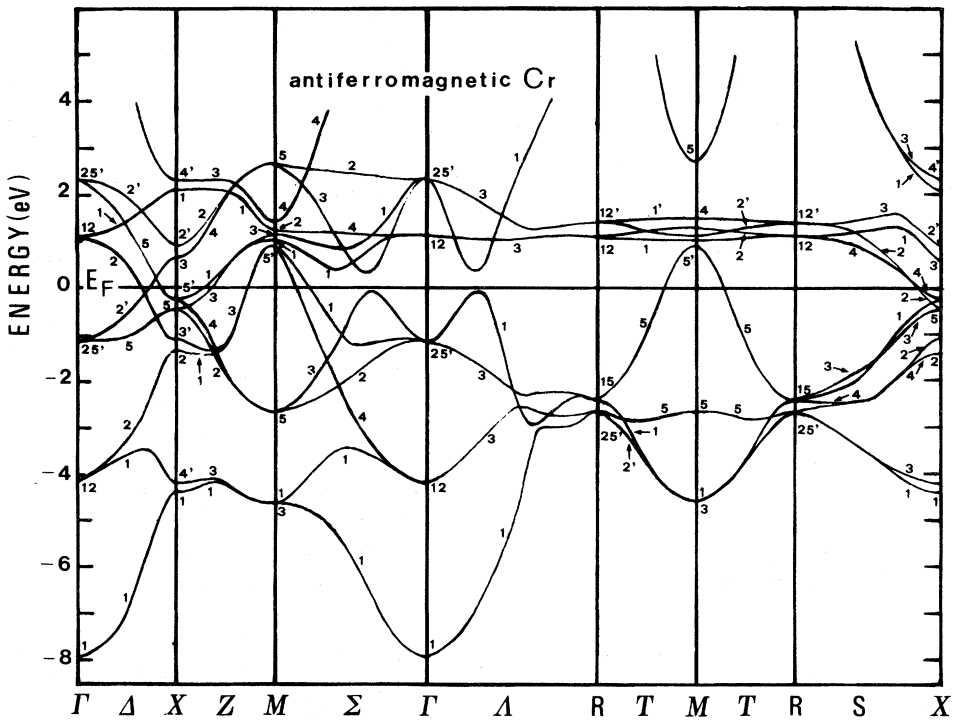

FIG. 4. Self-consistent band structure for the hypothetical commensurate antiferromagnetic phase of Cr, as calculated by Skriver (Ref. 23). No calculations are available for the incommensurate real antiferromagnetic state of Cr. Our low-temperature optical data have been interpreted within Skriver's calculations.

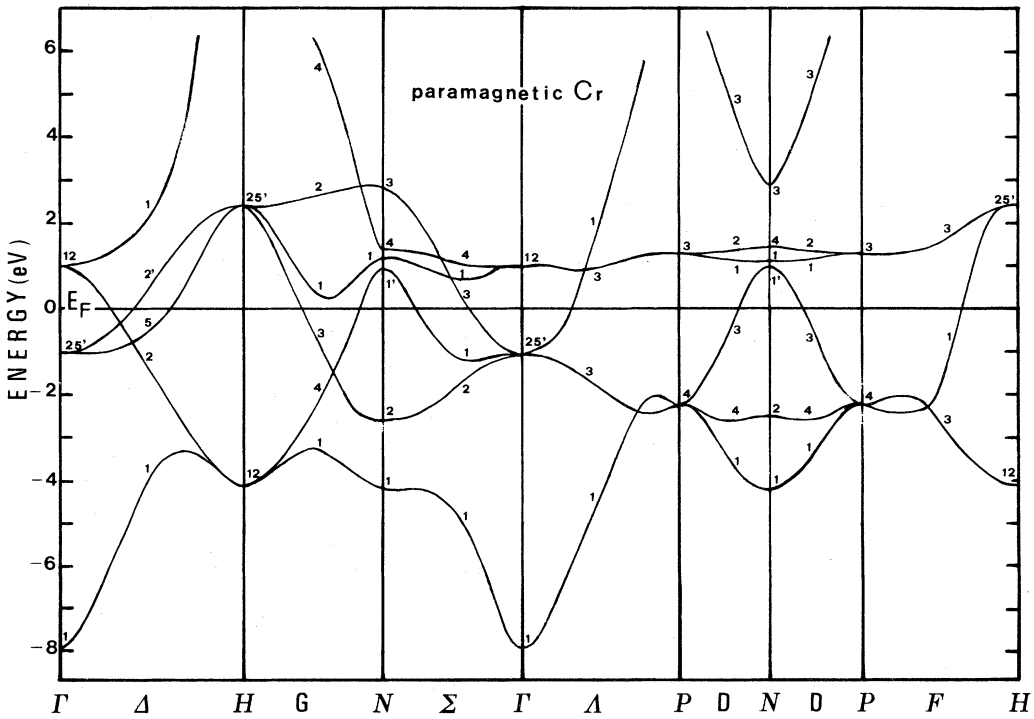

FIG. 5. Self-consistent band structure for paramagnetic Cr as calculated by Laurent *et al.* (Ref. 31). Our high-temperature optical data have been interpreted with the help of these calculations.

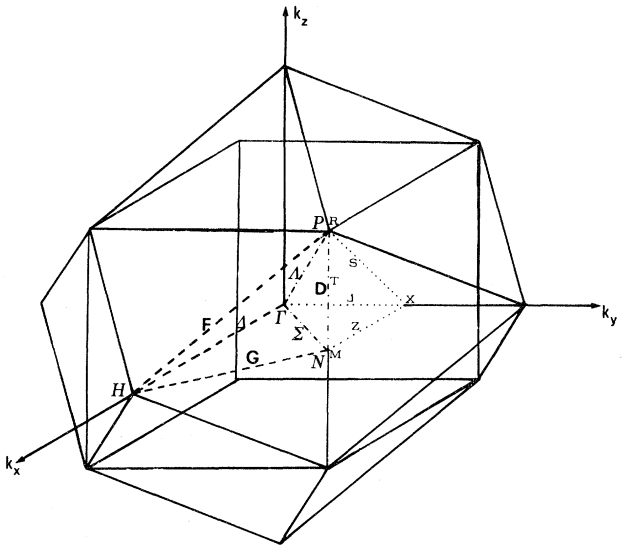

FIG. 6. bcc Brillouin zone (heavy solid lines) of paramagnetic Cr. The CsCl Brillouin zone of the hypothetical commensurate antiferromagnetic phase of Cr is shown for comparison (thin solid lines). The irreducible parts of both Brillouin zones are also sketched (dotted and dashed lines, respectively).

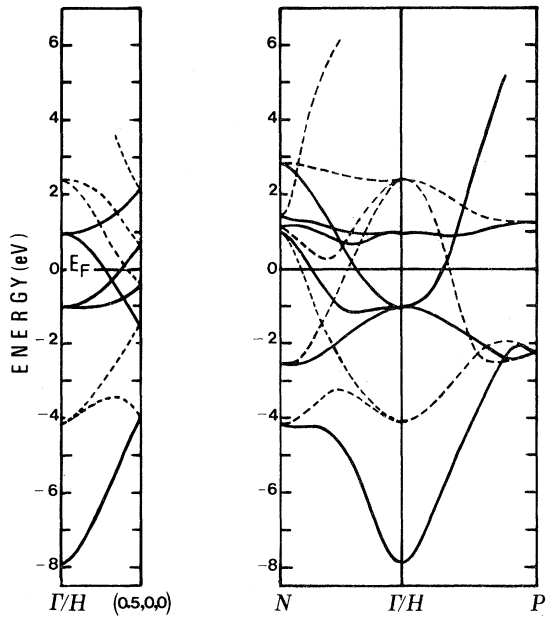

FIG. 7. Qualitative picture of the band structure for commensurate antiferromagnetic Cr. The structure was obtained folding back the bands of the paramagnetic state (Fig. 5) in the simple cubic Brillouin zone. This procedure is useful for understanding the origin of the energy levels in the antiferromagnetic band structure. While several energy levels are largely unaffected by the phase transition, turning on the antiferromagnetic interaction opens new gaps at the surface of the new Brillouin zone and accidental degeneracies are removed through the opening of gaps along Λ and Σ near the Fermi surface.

photon-energy range. We interpret these structures as deriving from optical transitions involving the Fermi surface. Qualitatively, a Fermi-surface transition shows a relatively sharp[42] derivativelike line shape.[27,43] The energy of the onset of the transition corresponds to the zero-crossing energy of the derivative $\Delta\epsilon_2$ line shape and to an absolute minimum in the corresponding $\Delta\epsilon_1$ line shape. Characteristically, $\Delta R/R$ also has a derivativelike lineshape where the onset is located in the neighborhood of the positive maximum. All these conditions are verified in the experimental spectra. As an example we show, in Fig. 9, a tentative decomposition of the three contributions to $\Delta\epsilon_2$. According to the sketch, the transitions are located at about 0.9, 1.4, and 1.6 eV and appear on a rapidly decreasing background (mainly determined by the free-electron contribution).

Several possible candidates exist for the observed Fermi-surface transitions. We expect important contributions[41] from transitions along Z, Σ, T, and S (see Table I). All these contributions are not affected by the magnetic phase transition and have to be taken into account in the interpretation of the experimental data for the paramagnetic case.

The higher-energy features in the $\Delta\tilde{\epsilon}$ spectra derive from critical-point contributions. These are expected to be dominant in the thermoreflectance spectrum,[27–29] together with Fermi-surface transitions. Four types of critical points are possible, each corresponding to a characteristic $\Delta\tilde{\epsilon}$ line shape.[27,32] In Fig. 10 we show a qualitative decomposition of the $\Delta\tilde{\epsilon}$ structures. A rigorous fitting of $\Delta R/R$ data in the (2—4)-eV photon-energy range is shown in Fig. 11. The analytical procedure[32,33] for reproducing the $\Delta R/R$ spectrum has been used several times[28,33] for supporting critical-point identifications and is standard by now. The agreement with experiment is remarkably good, even though the theory involves rather crude approximations,[44] and confirms the identifications[45] of Fig. 10. The fitting parameters are shown in Table II.

The critical points M_1 (at 1.95 eV) and M_3 (at 2.65 eV) correspond to transitions at the X point, namely $X'_5 \rightarrow X_1$, which exist only in the antiferromagnetic phase because of the opening of gaps along Δ. A careful look at the band-structure topology (Fig. 4) rules out different assignments. The experimentally determined M_2 critical point (at 2.37 eV) cannot occur at high-symmetry points in the BZ. On increasing the temperature above T_N we expect the M_1 and M_3 contributions to disappear gradually since they probably convert to noncritical interband transitions along Δ.

The M_2 contribution, instead, should remain relatively unaffected. Its most probable origin is along

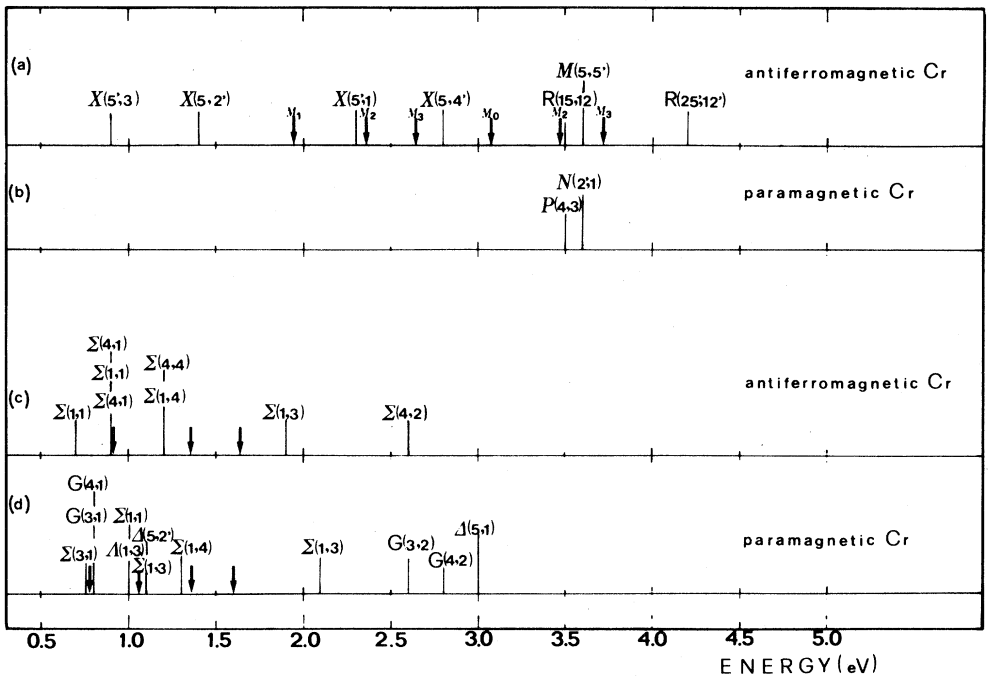

FIG. 8. Panel (a): Allowed critical-point transitions at high-symmetry points for antiferromagnetic Cr from the band structure of Fig. 4 through selection-rule and joint-density-of-states arguments. Panel (b): Allowed critical-point transitions at high-symmetry points for paramagnetic Cr. Panels (c) and (d): Main interband transitions (Ref. 41) involving final or initial states at the Fermi level for antiferromagnetic [panel (c)] and paramagnetic Cr [panel (d)]. Only transitions that should be affected by magnetic ordering (along the Λ, G, and Λ symmetry lines) are shown. The arrows indicate Fermi-surface and critical-point transitions determined experimentally.

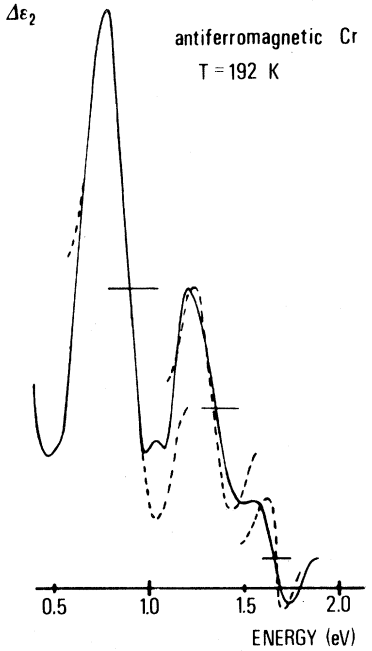

FIG. 9. Tentative decomposition of the low-energy region of the $\Delta\epsilon_2$ spectrum for antiferromagnetic Cr. Three Fermi-surface transitions on a rapidly decreasing free-electron background can account qualitatively for the observed line shapes.

Σ near M ($\Sigma_1 \rightarrow \Sigma_2$ transitions).

The M_3 contribution at 3.72 eV corresponds to interband transitions at the R and/or M symmetry points and should be present also in the paramagnetic phase, occurring at P and/or N. In fact, band-structure calculations show that the transition along the D-symmetry lines are not affected by magnetic ordering. This absorption feature is characteristic of the transition metals of the V (Ref. 29) and Cr (Ref. 46) groups and it is clearly detected in all these metals.

The origin of the M_0 and M_2 critical points at 3.08 and 3.48 eV is less clear, but they occur away from high-symmetry points. Transitions along T, Z, and Σ are likely candidates from energy-difference arguments. Along these directions we find pairs of bands almost unaffected by the magnetic phase transition. Therefore, they should also contribute to the optical spectra of paramagnetic Cr.

Comparison with paramagnetic Cr spectra can provide further support to our identifications. The theoretical trends described in the previous paragraphs will be used to lead the interpretation.

The thermoreflectance spectra of *bulk* Cr (Fig. 1) show important changes with magnetic ordering in the low-energy range ($h\nu \lesssim 1.5$ eV). Most of the

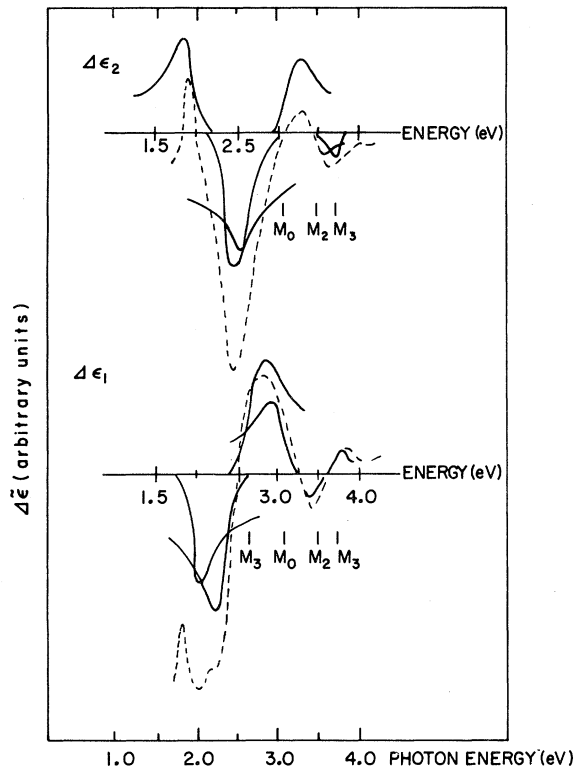

FIG. 10. Qualitative decomposition of the high-energy region of the $\Delta\tilde{\epsilon}$ spectra of antiferromagnetic Cr in terms of critical-point transitions. A corresponding rigorous fitting of the $\Delta R/R$ data is shown in Fig. 11.

other spectral features remain essentially unchanged. Figure 1 shows a gradual increase in magnetic ordering in the $\Delta R/R$ spectra. Although coherent spin-density waves disappear at T_N, paramagnons persist at temperatures considerably higher.[47] Therefore, the $\Delta R/R$ spectrum at 325±3 K (only 13±6 K above T_N), may not be representative of the pure paramagnetic phase.

Weaver *et al.* performed thermoreflectance measurements[36] on Cr films well above and below T_N (340 and 80 K) and did not observe any change

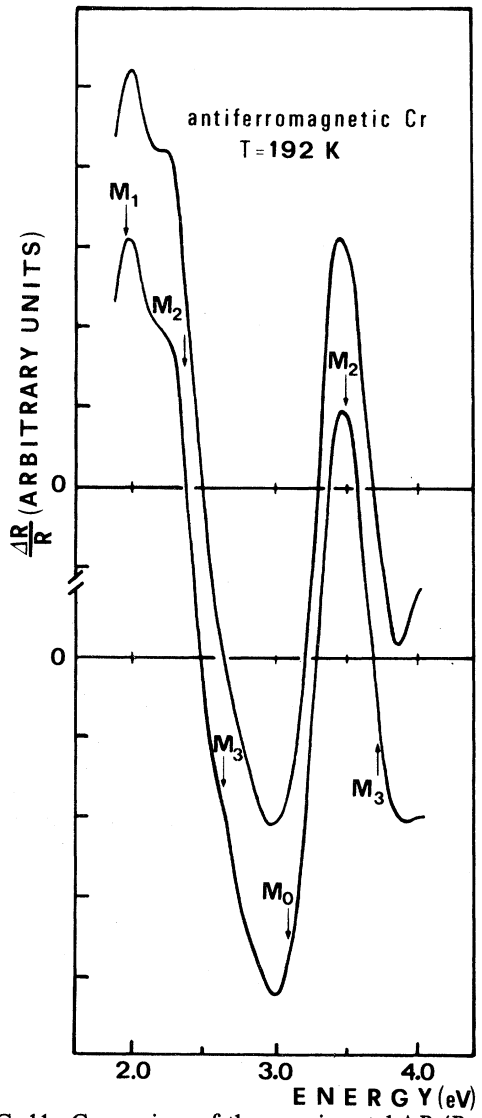

FIG. 11. Comparison of the experimental $\Delta R/R$ spectrum of antiferromagnetic Cr with the result of an analytical fitting (Refs. 32 and 33) based on the qualitative identification of Fig. 10. The agreement is remarkably good, even though the theory involves rather crude approximations (Ref. 44). The fitting parameters are shown in Table II.

TABLE III. Parameters used in the analytical fitting of the experimental $\Delta R/R$ spectrum of Cr films (see Fig. 13). Because the experimental curve is less structured than the antiferromagnetic $\Delta R/R$ curve the fitting parameters are less precise: The energy location of the critical point is reliable to within ±0.07 eV and the broadening parameters to within ±5%. W is a phenomenological weight parameter proportional to $J\Gamma^{-1/2}|M|^2|\Delta E_0|$, where J is a topological factor, ΔE_0 is the temperature-induced modulation of the energy gap, and M is the transition matrix element.

Critical point	M_2	M_0	M_2	M_3
Onset E_0 (eV)	2.30	2.84	3.42	3.66
Broadening Γ (eV)	0.35	0.41	0.25	0.27
Weight W (eV^2)	9.90	8.70	1.30	3.40

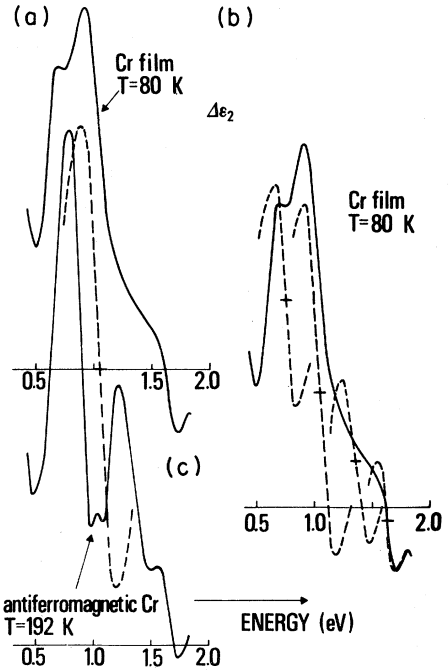

FIG. 12. Low-energy region of the $\Delta\tilde{\epsilon}$ spectra for Cr films (a). The spectrum can be reproduced qualitatively by adding to the antiferromagnetic $\Delta\tilde{\epsilon}$ spectra the line shape of a new Fermi-surface transition at ~ 1.0 eV [(b) and (c)].

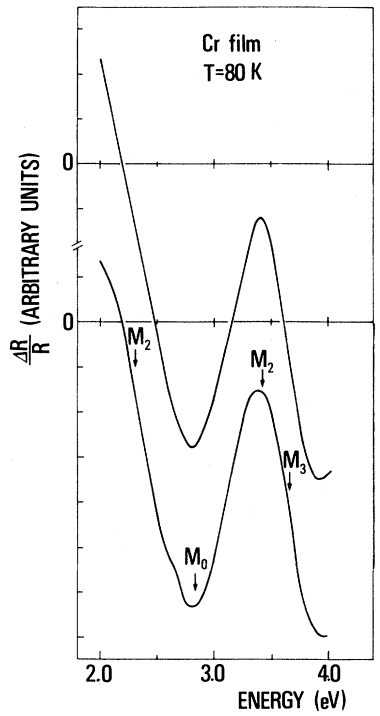

FIG. 13. Comparison of the experimental $\Delta R/R$ spectrum of Cr films with the result of an analytical fitting (Refs. 32 and 33) of the spectrum in terms of four critical-point contributions. (The fitting parameters are shown in Table III.) The remarkably good agreement of theory and experiment, together with the analysis of the systematic trends of the optical properties of the Cr-group metals (Ref. 46), confirms our assignments.

correlated with magnetic ordering. The $\Delta R/R$ spectrum of Cr films at 80 K (Fig. 1) does not show any feature characteristic of antiferromagnetic bulk Cr. The results of Weaver *et al.* seem not to depend on the antiferromagnetic interaction and to be representative, instead, of the pure paramagnetic state.[48]

The low-energy region of the $\Delta\tilde{\epsilon}$ spectra for Cr films (Figs. 2 and 3) is reproduced in Fig. 12. The experimental line shape is not easily recognizable as due to Fermi-surface transitions, unlike the antiferromagnetic case. We obtain, however, remarkably good agreement with experiment (see sketch in Fig. 12) by adding to the antiferromagnetic spectrum the line shape of a new Fermi-surface transition at ~ 1.0 eV. This was suggested by the theoretical analysis mentioned above. Figure 12(a) supports the quantitative decomposition of the paramagnetic $\Delta\epsilon_2$ spectrum shown in Fig. 12(b). All the Fermi-surface transitions identified so far are shown by arrows in Fig. 8 [panels (c) and (d)].

The Fermi-surface transitions at about 1.0 eV disappear when the antiferromagnetic interaction is switched on. Therefore, they are located along the symmetry directions affected by magnetic ordering.[23] From Fig. 8 we see that $\Sigma_1 \rightarrow \Sigma_3$ (E_F) and Λ_1 $(E_F) \rightarrow \Lambda_3$ transitions are the most likely candidates. A more comprehensive view of Fig. 8 [panels (a) and (c)] also reveals a theoretical critical-point transition $(X'_5 \rightarrow X_3)$ at about 1.0 eV. This contribution should be present only in the antiferromagnetic phase and replaces somewhat the Fermi-surface transition which disappears when the antiferromagnetic interaction is switched on.

The other Fermi-surface transitions are almost unaffected by magnetic ordering, keeping in mind the change of symmetry. The transitions G_4 $(E_F) \rightarrow G_1$ which occur at 0.8 eV in paramagnetic Cr become Σ_4 $(E_F) \rightarrow \Sigma_1$ in the antiferromagnetic phase and shift to slightly higher energy.

Returning to the higher-energy spectral range, we previously identified several critical-point absorption features in the antiferromagnetic Cr spectrum [Fig. 8, panel (a)]. An M_0- and two M_2-type absorption features were identified as corresponding to symmetry lines of the BZ where they should not be affected by magnetic ordering. Of the other three critical-point absorption features, two (M_1 and M_3 types) occur at X and should completely disappear in the

paramagnetic phase while the last M_3-type critical point (at R and/or M) should survive the magnetic phase transition [see Fig. 8, panel (b)]. Therefore, in the (2.0—4.0)-eV photon-energy range the $\Delta R/R$ spectrum of paramagnetic Cr should exhibit only contributions along symmetry lines (M_2, M_0, and M_2) plus one M_3-type contribution at the N and/or P high-symmetry point.

Figure 13 shows a comparison of the experimental $\Delta R/R$ spectrum with the "analytical" $\Delta R/R$, as obtained through a fitting of the four different critical-point contributions. (The fitting parameters are shown in Table III.) The remarkably good agreement of theory and experiment is the most convincing argument in favor of our assignments. These results have also been tested through the systematic trend of optical properties of the metals of the Cr group.[46]

VI. CONCLUSION

Thermoreflectance has been shown to be a unique tool for investigating magnetic ordering in Cr. Our approach has been twofold: First, we analyzed the optical spectra in terms of the most recent band-structure calculations. Second, we probed the identifications through the magnetic phase transition. The analysis of the spectral changes, vis-à-vis the expected band-structure modifications, allowed us to make most identifications unambiguous.

In conclusion, most of the optical thermomodulation spectral features in the (0.5—5.0)-eV photon-energy range have a convincing interpretation. In the (2.0—4.0)-eV photon-energy range, the experimental spectra have been reproduced with an analytical model with strikingly good agreement between theory and experiment.

ACKNOWLEDGMENT

The Ames Laboratory is operated for the U. S. Department of Energy by Iowa State University under Contract No. W-7405-Eng-82. This work was supported by the Director for Energy Research, Office of Basic Energy Sciences.

[1]C. G. Shull and M. K. Wilkinson, Rev. Mod. Phys. 25, 100 (1953).
[2]W. M. Lomer, Proc. Phys. Soc. London 80, 489 (1962).
[3]A. W. Overhauser, Phys. Rev. Lett. 4, 462 (1960); Phys. Rev. 128, 1437 (1968).
[4]C. Herring, in *Magnetism,* edited by G. Rado and H. Suhl (Academic, New York, 1966), Vol. 4.
[5]S. Asano and J. Yamashita, J. Phys. Soc. Jpn. 23, 714 (1967).
[6]A. S. Barker, Jr., B. J. Halperin, and T. M. Rice, Phys. Rev. Lett. 20, 384 (1968).
[7]L. W. Bos, D. W. Lynch, and J. L. Stanford, Phys. Lett. 30A, 17 (1969).
[8]A. S. Barker, Jr. and J. A. Ditzenberger, Phys. Rev. B 1, 4378 (1970).
[9]L. W. Bos and D. W. Lynch, Phys. Rev. B 2, 4567 (1970).
[10]M. A. Lind and J. L. Stanford, Phys. Lett. 39A, 5 (1972).
[11]J. Rath and J. Callaway, Phys. Rev. B 8, 5398 (1973).
[12]A. Kotani, J. Phys. Soc. Jpn. 37, 1493 (1974).
[13]D. W. Lynch, R. Rosei, and J. H. Weaver, Phys. Status Solidi A 27, 515 (1975).
[14]In the commensurate antiferromagnetic structure the spins at the corner and at the center of the bcc unit cell are of equal magnitude and point in opposite directions. G. Shirane and W. J. Takei, J. Phys. Soc. Jpn., Suppl. 17, 35 (1962).
[15]W. C. Koehler, R. M. Moon, A. L. Trego, and A. R. Mackintosh, Phys. Rev. 151, 405 (1966).
[16]M. Asdente and J. Freidel, Phys. Rev. 124, 384 (1961).
[17]M. Asdente, Phys. Rev. 127, 1949 (1962).
[18]T. L. Loucks, Phys. Rev. 134, A1181 (1965).
[19]M. Yasui, E. Itayashi, and M. Shimizu, J. Phys. Soc. Jpn. 29, 1440 (1970).
[20]R. P. Gupta and S. K. Sinha, Phys. Rev. B 3, 2401 (1971).
[21]J. L. Fry, N. E. Brener, J. L. Thompson, and P. H. Dickinson, Phys. Rev. B 21, 384 (1980).
[22]J. Kübler, J. Magn. Magn. Mater. 20, 277 (1980).
[23]H. L. Skriver, J. Phys. F 11, 97 (1981).
[24]The slight difference between the hypothetical commensurate and incommensurate phases of Cr should produce only small differences in the eigenvalues $E(\vec{K})$ of the ground state (Ref. 23).
[25]The antiferromagnetic ordering gives rise to a CsCl-like structure where the simple cubic Brillouin zone has one-half the volume of the original bcc BZ.
[26]M. Cardona, in *Solid State Physics,* edited by F. Seitz, D. Turnbull, and H. Ehrenreich (Academic, New York, 1969), Suppl. 11.
[27]E. Colavita, S. Modesti, and R. Rosei, Phys. Rev. B 14, 4315 (1976).
[28]E. Colavita, A. Franciosi, R. Rosei, F. Sacchetti, E. S. Giuliano, R. Ruggeri, and D. W. Lynch, Phys. Rev. B 20, 4864 (1979).
[29]R. Rosei, E. Colavita, A. Franciosi, J. H. Weaver, and D. T. Peterson, Phys. Rev. B 21, 3152 (1980).
[30]L. I. Johansson, L. G. Peterson, K. F. Berggren, and J. W. Allen, Phys. Rev. B 22, 3294 (1980).
[31]D. G. Laurent, J. Callaway, J. L. Fry, and N. E. Brener, Phys. Rev. B 23, 4977 (1981), and references therein.
[32]B. Batz, in *Semiconductors and Semimetals,* edited by R. K. Willardson and A. C. Beer (Academic, New York, 1972), Vol. 9, p. 316.
[33]E. Colavita, G. Paolucci, and R. Rosei, Phys. Rev. B (in

press).

[34]The heating system is the now-standard high-efficiency arrangement successfully used in a number of thermoreflectance studies (Refs. 28, 29, 33, and 35).

[35]E. Colavita, G. Falasca, G. Paolucci, and R. Rosei (unpublished).

[36]J. H. Weaver, D. W. Lynch, C. H. Culp, and R. Rosei, Phys. Rev. B 14, 459 (1976).

[37]Spectra taken between 150 and 190 K do not show appreciable differences.

[38]Exponential tails have been used below 0.5 eV and above 5.0 eV. It has been checked that such extrapolations do not affect critically our analysis. See also A. Balzarotti, E. Colavita, S. Gentile, and R. Rosei, Appl. Opt. 14, 2412 (1975).

[39]The measured (Ref. 9) dielectric function $\tilde{\epsilon}(\omega)$ is, in fact, almost identical for antiferromagnetic and paramagnetic Cr in the (0.5—5.0)-eV photon-energy range, indicating the rather poor sensitivity of static optical techniques to the magnetic ordering effects in this photon-energy range.

[40]J. E. Nestell, Jr. and R. W. Christy, Phys. Rev. B 21, 3173 (1980).

[41]From joint-density-of-states and selection-rule arguments.

[42]The typical distance between the positive and negative peaks is of the order of $5kT$.

[43]R. Rosei, Phys. Rev. B 10, 474 (1974); R. Rosei, C. H. Culp, and J. H. Weaver, *ibid.* 10, 484 (1974); M. Guerrisi, R. Rosei, and P. Winsemius, *ibid.* 12, 557 (1975).

[44]The crudest approximation is probably the assumption of a constant dipole matrix element in the neighborhood of each critical point.

[45]The simultaneous analysis of the $\Delta\epsilon_1$, $\Delta\epsilon_2$, and $\Delta R/R$ spectra makes unambiguous the critical-point identification. Many different attempts have been performed to obtain a fit of the $\Delta R/R$ spectrum in the high-energy range ($h\nu \geq 3$ eV). The M_0, M_2, and M_3 critical points (which are not easily recognizable in $\Delta\tilde{\epsilon}$) were found to be essential for reproducing the $\Delta R/R$ spectrum. The M_2 contribution at about 3.5 eV is small in $\Delta\tilde{\epsilon}$. However, it accounts for a dominant positive lobe in the $\Delta R/R$ spectrum because of an amplification effect from the Seraphin coefficients.

[46]E. Colavita, A. Franciosi, C. Mariani, and R. Rosei (unpublished).

[47]S. K. Sinha, S. H. Liu, L. D. Muhlestein, and N. Wakabayashi, Phys. Rev. Lett. 23, 311 (1969). Paramagnons, however, should exist with a much broader spectrum of wave vectors, broadening considerably any gaps present above T_N due to the incipient magnetic ordering.

[48]Without a structural characterization of the evaporated samples one can only speculate on the importance of structural disorder in opposing the formation of the spin-density-wave long-range periodicity. Strain effects in evaporated films may broaden considerably the experimental optical features, but cannot account for the systematic trends in Fig. 1.